

A non-invasive fault location method for modular multilevel converters under light load conditions

Yaqian Zhang¹, Yi Zhang^{2,3}, Frede Blaabjerg², Jianzhong Zhang¹

1. School of Electrical Engineering, Southeast University, Nanjing, China

2 AAU Energy, Aalborg University, Aalborg, Denmark

3 Swiss Federal Institute of Technology Lausanne (EPFL), Lausanne, Switzerland
(yaqianzhang83@seu.edu.cn, yiz@energy.aau.dk, fbl@energy.aau.dk, jiz@seu.edu.cn)

Abstract—This paper proposes a non-invasive fault location method for modular multilevel converters (MMC) considering light load conditions. The prior-art fault location methods of the MMC are often developed and verified under full load conditions. However, it is revealed that the faulty arm current will be suppressed to be unipolar when the open-circuit fault happens on the submodule switch under light load. This leads to the capacitor voltage of the healthy and faulty submodules rising or falling with the same variations, increasing the difficulty of fault location. The proposed approach of injecting the second-order circulating current will rebuild the bipolar arm current of the MMC and enlarge the capacitor voltage deviations between the healthy and faulty SMs. As a result, the fault location time is significantly shortened. The simulations are carried out to validate the effectiveness of the proposed approach, showing that the fault location time is reduced to 1/6 compared with the condition without second-order circulating current injection.

Keywords—Circulating current injection, Fault location, Light load, Modular multilevel converter, Open-circuit fault.

I. INTRODUCTION

The modular multilevel converter (MMC) is one of the most promising multilevel converters in high-voltage applications thanks to the modularity, superior AC performance, and scalability to meet any voltage level [1]. The half-bridge (HB) submodule (SM) has the simplest structure and lowest power losses, becoming the most popular SM for the MMC. In general, there are even hundreds of identical SMs and massive power switching devices in the MMC, which have a high malfunction rate threatening the reliability of the MMC [2]. Therefore, it is necessary to detect and locate the fault quickly so that further measurements can be taken to protect the MMC from being broken down.

Open-circuit and short-circuit are two typical faults of power semiconductor switches. The short-circuit fault detection is easier and faster to be realized by the switch level circuit, which is usually embedded into the commercial gate driver circuit [3]. However, the open-circuit fault would not cause obvious damage immediately; instead, it remains undetected for a relatively long time and cause a subsequent influence on the overall MMC system [4]. Once an open-circuit fault happens in one or multiple SMs, the output performance of the MMC will deteriorate because the actual output voltage of the faulty SM does not match the required output modes. Moreover, the capacitor in a faulty SM will be overcharged if the faulty SM is not detected and isolated in time. Then the capacitor voltage will be increased to exceed the safe threshold and, at last, break down the whole MMC system [5].

The existing methods of faulty SM location for the MMC are mainly classified into two types, i.e., the hardware-based and software-based methods.

The hardware-based method can realize the fault location within short time. In [6], the voltage sensor is employed to measure the arm voltage and detect the faulty arm. However, it can only be used to locate the defective arm, not the faulty SM. Two voltage sensors are used in each SM in [7] to accurately locate the faulty SM. One voltage sensor is parallel with the capacitor to realize the voltage balancing control, and the other is paralleled to the lower power switch to detect the SM output voltage and compared with the reference switching signal. However, the cost is significantly increased since the number of SMs is usually large. In [8], the two voltage sensors are reduced to one in each SM and the voltage sensor is re-configured to be parallel connected with the upper power switch. The cost is not increased, but the extra voltage observer is required to acquire the capacitor voltage, making the control more complex. Moreover, the above voltage observer will lose the accuracy with the SM capacitance aging, negatively affecting the normal MMC operation. Therefore, with respect to the system cost and operation robustness, the hardware-based approaches of faulty SM location in [7] and [8] are not the best choice.

The software-based methods are proposed for the HBSM MMC without changing the converter structure or sensor configuration. There are three types of software-based methods, namely the signal-based methods, model-based methods, and data-based methods. In the signal-based methods [9], the detected signal is compared with the reference signal, and the fault can be located once the signal deviation exceeds the threshold and last for a certain time. In model-based methods [10], voltage or state observers are demanded to compare the estimated and actual values. Besides, an appropriate threshold is required but difficult to satisfy the requirements under different power levels. In the data-based methods [11], the data feature of the SM capacitor voltage is extracted to detect the error data and derive the error possibility. However, this method depends on the capacitor voltage deviations between the faulty and healthy SMs. Above all, all the aforementioned software-based approaches perform well under the rated power level but are not evaluated under light load conditions.

The arm current will be distorted to be unipolar or even zero by the SM open-circuit faults when the MMC operates under light load [12]. In this case, the capacitor voltage of the healthy and faulty SMs will vary similarly, and the voltage deviations are quite small or even disappear. This will cause the failure of the existing software-based methods since they are all achieved by extracting the capacitor voltage difference between the healthy and faulty SMs.

The fault location of MMC under the light load condition is considered in literature [12], where the hardware-based method is adopted to detect the faulty SM. The bleeding resistor is re-arranged and auxiliary circuits are equipped for

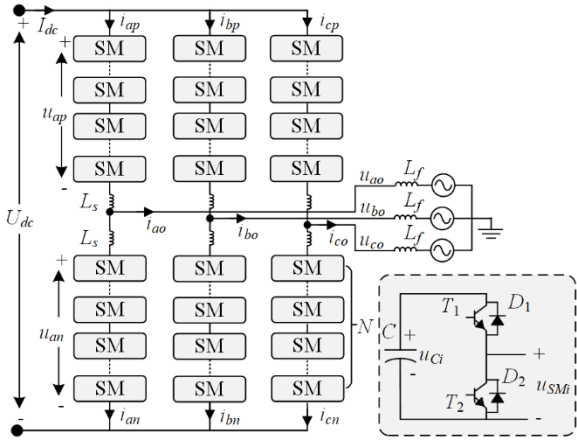


Fig. 1. Configuration of three-phase MMC.

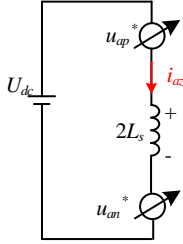


Fig. 2. Equivalent circuit on DC side under normal state.

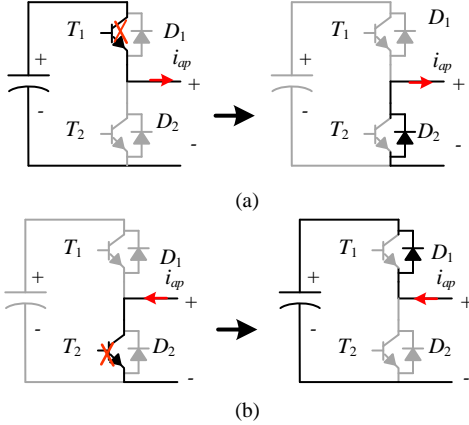


Fig. 3. Open-circuit fault in SM of faulty (a) T_1 , (b) T_2 .

each SM to detect the output voltage of the SM in real-time. However, the system costs are increased since the number of SMs is large for the MMC system.

In this paper, a software-based fault location method is proposed for the MMC under light load condition to accelerate the fault location speed. First, the mechanism of the unipolar arm current under fault is analyzed and the approximate criterion of high risk of unipolarity is derived. Second, the circulating current injection is enabled after the faulty arm is detected so that the arm current recovers to the bipolar variations. The amplitude and phase of the reference second-order circulating current are selected for different types of faults. Then the capacitor voltage deviations between the faulty and healthy SMs are appropriately enlarged to shorten the fault location time.

II. OPEN-CIRCUIT FAULT OF MODULAR MULTILEVEL CONVERTERS

A. Configuration of MMC

Table I. States of Healthy SM

Mode	i_{ap}	S_{api}	State	Path	u_{SMi}	u_{Ci}
1	≥ 0	1	Insert	D_1	$+u_{Ci}$	Increase
2	≥ 0	0	Bypass	T_2	0	Unchanged
3	< 0	1	Insert	T_1	$+u_{Ci}$	Decrease
4	< 0	0	Bypass	D_2	0	Unchanged

Table II. Two types of Open-circuit Fault

Fault type	Mode	i_{ap}	S_{api}	State	u_{SMi}	u_{Ci}
T_1 fault	1	≥ 0	1	Insert	$+u_{Ci}$	Increase
	2	≥ 0	0	Bypass	0	Unchanged
	3	< 0	1	Bypass	0	Unchanged
	4	< 0	0	Bypass	0	Unchanged
T_2 fault	1	≥ 0	1	Insert	$+u_{Ci}$	Increase
	2	≥ 0	0	Insert	$+u_{Ci}$	Increase
	3	< 0	1	Insert	$+u_{Ci}$	Decrease
	4	< 0	0	Bypass	0	Unchanged

Fig. 1 shows the configuration of the three-phase MMC, where each phase consists of upper and lower arms. Each arm contains one arm inductor and N identical HBSMs. In each HBSM, u_{Ci} represents the capacitor voltage. u_{SMi} is the output voltage of the SM, having $+u_{Ci}$ and 0, namely the insert and bypass states, respectively. i is the numbering of each SM in each arm, having $i=1, \dots, N$. u_{xy} denotes the summation of HBSM output voltage in the y arm of phase x , where $x=a, b, c, y=p, n$.

Since the HBSM can only output nonnegative voltage, the charging or discharging states of the SM capacitor are determined by the arm current, which is shown in Table I. When the arm current is positive, the SM is inserted via D_1 and bypassed via T_2 . When the arm current is negative, the SM is inserted by T_1 and bypassed by D_2 .

The arm voltage and current of each arm are expressed as

$$\begin{cases} u_{xy} = \frac{U_{dc}}{2} \mp U_m \sin(\omega t + \varphi_x) \\ i_{xy} = \frac{I_{dc}}{3} \pm I_m \sin(\omega t + \varphi_x + \varphi) \end{cases} \quad (1)$$

where only DC and fundamental components are included in the arm currents with the higher-order currents suppressed. According to the power balancing between the DC and AC sides, the DC and AC current have the relations of

$$I_{dc} = \frac{3m}{4} I_m \cos \varphi \quad (2)$$

where φ is the power factor angle of the MMC. m is the modulation index of the MMC, having $U_m/(U_{dc}/2)$.

Taking phase a as an example and seeing from the DC side, the equivalent circuit of the MMC can be illustrated in Fig. 2. We have

$$U_{dc} - (u_{ap} + u_{an}) = 2L_s \frac{di_{az}}{dt} \quad (3)$$

where i_{az} is the circulating current between the DC side and phase a . Under the normal operations in Fig. 3, the actual u_{ap} and u_{an} follow the required reference value u_{ap}^* and u_{an}^* , respectively. u_{ap}^* and u_{an}^* have

$$U_{dc} - (u_{ap}^* + u_{an}^*) = 0 \quad (4)$$

Then the right term of (1) is zero without fault occurrence, which is

$$2L_s \frac{di_{az}}{dt} = 0 \quad (5)$$

which is consistent with the fact that the circulating current is controlled as the DC component under normal operation.

B. Open-circuit Fault

Fig. 3 shows two types of open-circuit faults on T_1 and T_2 . In Fig. 3(a), the SM cannot be inserted under $i_{ap} < 0$ when the upper switch T_1 is faulty, and the arm current can only flow through the freewheeling diode D_2 . Therefore, as shown in Table II, the faulty SM cannot be discharged in Mode 3, leading to over-voltage of the SM capacitor. In Fig. 3(b), the SM cannot be bypassed by T_2 under $i_{ap} > 0$ with open-circuit occurrence on T_2 . In this case, the arm current flows via the freewheeling diode D_1 and charges the SM capacitor. As a result, the capacitor voltage of the faulty SM keeps increasing as shown in mode 2 of T_2 fault in Table II. This will also cause over-voltage of the faulty SM.

Based on the above analysis, the open-circuit fault of T_1 or T_2 will both cause an abnormal increase and divergence of the corresponding SM capacitor voltage. Also, as the faulty SM cannot output the voltage required by the switching signal, the arm voltage is distorted, causing circulating and arm current distortion. This fault of arm current or circulating current is used to detect the faulty arm or phase. But the specific faulty SM must be located by distinguishing its own capacitor voltage or other information inside each SM.

III. IMPACT OF LIGHT LOAD ON IGBT OPEN-CIRCUIT FAULT LOCATION

This section clarifies the impact of the system parameters and operation conditions on the faulty arm current polarities. It emphasizes the negative impact of neglecting the light load condition on the fault location of the MMC.

A. Unipolar arm current under T_1 fault

Assume that the faulty SM exist in the upper arm. Under the open-circuit fault of T_1 , SM1 cannot be inserted but only be bypassed by the diode D_2 with $i_{ap} < 0$. Then the actual arm voltage is smaller than the reference arm voltage, which is

$$u_{ap_f1} = \begin{cases} u_{ap}^* - S \cdot U_c & i_{ap} < 0 \\ u_{ap}^* & i_{ap} > 0 \end{cases} \quad (6)$$

where S is the reference switching function of the faulty SM, having $S=0,1$.

Fig. 4 illustrates the equivalent circuit under T_1 fault. The voltage deviation under T_1 fault is given by

$$\Delta u_{ap_f1} = u_{ap}^* - u_{ap_f1} = \begin{cases} S \cdot U_c & i_{ap} < 0 \\ 0 & i_{ap} > 0 \end{cases} \quad (7)$$

Here we assume that the faulty SM capacitor voltage is not changed too much and is still limited to the safety zone without over-voltage before it is located. In Fig. 4(c), Δu_{ap_f1} is evenly distributed on the two arm inductors. Then the faulty current component under T_1 is

$$\Delta i_{ap_f1} = \int \frac{S \cdot U_c}{2L_s} dt \quad i_{ap} < 0 \quad (8)$$

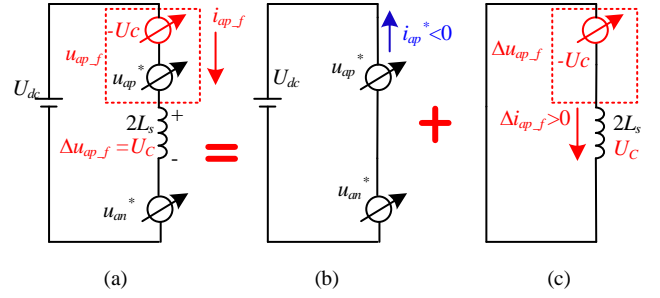


Fig. 4. Equivalent circuit of T_1 fault. (a) Overall circuit. (b) Normal part. (c) Faulty part.

In Fig. 4(a), the faulty arm current i_{ap_f1} is composed of the normal component i_{ap}^* and the faulty component Δi_{ap_f} , which is given as

$$i_{ap_f1} = \Delta i_{ap_f1} + i_{ap}^* \quad i_{ap_f1} < 0 \quad (9)$$

Since the faulty component in (8) is positive, the negative part of the arm current becomes smaller under the open-circuit fault. In particular, the negative part of i_{ap_f1} might disappear under light load.

If the following prerequisite is satisfied, the negative part of the arm current will be canceled out, leading to the unipolar faulty arm current with only the nonnegative part.

$$\Delta i_{ap_f} \geq \max(|i_{ap}^*|) \quad i_{ap} < 0 \quad (10)$$

Combining (10) with (1), we have

$$\max(|i_{ap}^*|) = \frac{I_m}{2} - \frac{I_{dc}}{3} \quad i_{ap} < 0 \quad (11)$$

Combining (2), (8) and (11), the criterion in (10) is given as

$$\int (S) dt \geq \left(\frac{1}{2} - \frac{m \cos \varphi}{4} \right) \frac{2I_m L_s}{U_c} \quad (12)$$

To make sure that (12) is satisfied, the left term is suppressed as the integration of one switching period, which is approximated as

$$\int (S) dt = \left(\frac{1}{2} - \frac{m}{2} \sin(\omega t) \right) \cdot \Delta T_c \approx \frac{1}{2f_c} \quad (13)$$

where f_c is the carrier and switching frequency.

Combining (12) and (13), the critical condition to generate the unipolar arm current is expressed as

$$I_m = \frac{U_{dc}}{(2 - m \cos \varphi)} \cdot \frac{1}{Nf_c L_s} \quad (14)$$

In case of the multiple faulty SMs, N_{f1} refers to the number of SMs with T_1 fault. Then (14) is written as

$$I_m = \frac{U_{dc} \cdot N_{f1}}{(2 - m \cos \varphi)} \cdot \frac{1}{Nf_c L_s} \quad (15)$$

which means that, if the AC current amplitude is lower than the right side, the faulty arm current will become nonnegative. As a result, all the SMs cannot be discharged and have the same voltage variations as the faulty SM1. This will cause the failure to locate the faulty SM quickly.

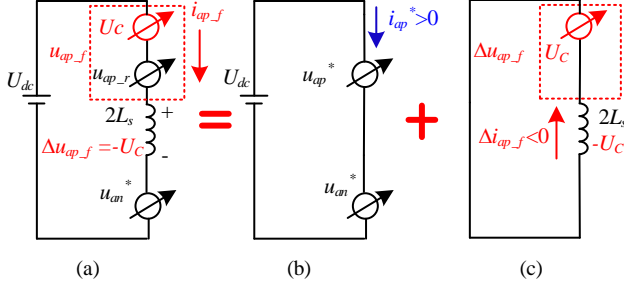


Fig. 5 Equivalent circuit of T_2 fault. (a) Overall circuit. (b) Normal part. (c) Faulty part.

Table III Cases of different impact factors

Impact factors	Case	Parameters
Arm inductance L_s	1	$L_s=8\text{mL}$, $\cos\varphi=1$, $f_c=1.2\text{ kHz}$, $m=0.9$
	2	$L_s=5\text{mL}$, $\cos\varphi=1$, $f_c=1.2\text{ kHz}$, $m=0.9$
Modulation index m	3	$L_s=8\text{mL}$, $\cos\varphi=1$, $f_c=2\text{ kHz}$, $m=0.9$
	4	$L_s=8\text{mL}$, $\cos\varphi=1$, $f_c=2\text{ kHz}$, $m=0.8$
Power factor $\cos\varphi$	5	$L_s=8\text{mL}$, $\cos\varphi=1$, $f_c=1.2\text{ kHz}$, T_1
	6	$L_s=8\text{mL}$, $\cos\varphi=0.86$, $f_c=1.2\text{ kHz}$, T_2
Number of faulty SMs N_{f1}, N_{f2}	7	$L_s=8\text{mL}$, $\cos\varphi=0$, $f_c=1.2\text{ kHz}$, $N_{f1}=1$
	8	$L_s=8\text{mL}$, $\cos\varphi=0$, $f_c=1.2\text{ kHz}$, $N_{f1}=2$
	9	$L_s=8\text{mL}$, $\cos\varphi=0$, $f_c=1.2\text{ kHz}$, $N_{f1}=3$

B. Unipolar arm current under T_2 fault

If T_2 suffers from the open circuit fault, SM1 cannot be bypassed under $i_{ap}>0$ and then the actual arm voltage u_{ap} becomes

$$u_{ap-f2} = \begin{cases} u_{ap}^* + S \cdot U_c & i_{ap} > 0 \\ u_{ap}^* & i_{ap} < 0 \end{cases} \quad (16)$$

As seen from the equivalent circuit in Fig. 5, the faulty arm voltage deviation under T_2 fault is

$$\Delta u_{ap-f2} = u_{ap}^* - u_{ap-f2} = \begin{cases} -(1-S) \cdot U_c & i_{ap} > 0 \\ 0 & i_{ap} < 0 \end{cases} \quad (17)$$

which is imposed on the arm inductors and generates the faulty component of the arm current:

$$\Delta i_{ap-f2} = \int \frac{(S-1) \cdot U_c}{2L_s} dt \quad i_{ap} > 0 \quad (18)$$

which is negative under the positive arm current. It means that the faulty component is always opposite to the normal component, then the positive interval of the arm current will be cut off, even causing unipolarity.

Similar to the analysis of the T_1 fault, the unipolar arm current under T_2 fault occurs under the following conditions:

$$I_m = \frac{U_{dc} \cdot N_{f2}}{(2 + m \cos \varphi)} \cdot \frac{1}{N_f L_s} \quad (19)$$

where N_{f2} is the number of SMs with T_2 fault. It means that when the AC current amplitude is lower than the right term, then there will be high possibility of nonpositive arm current.

In (15) and (19), it shows that whether the faulty arm current will become unipolar is affected by various factors, i.e., the number of SMs when the DC bus voltage is fixed, the power/current level, the arm inductance, the carrier frequency,

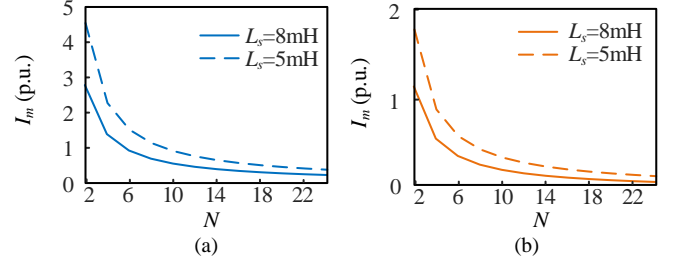


Fig. 6 Impact of arm inductance on faulty arm current. (a) T_1 fault. (b) T_2 fault. (Case 1 and case 2).

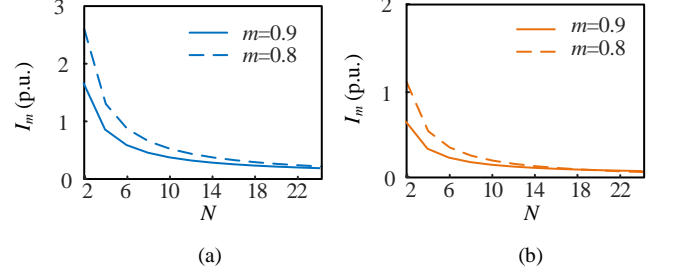


Fig. 7 Impact of modulation index on faulty arm current. (a) T_1 fault. (b) T_2 fault. (Case 3 and case 4).

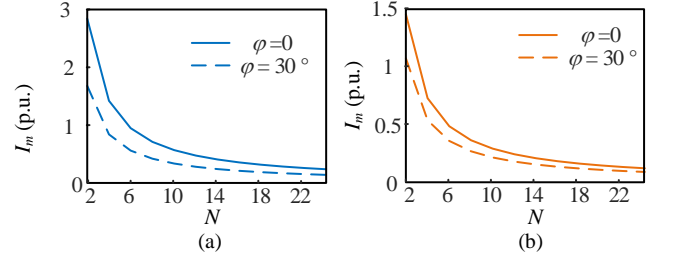


Fig. 8 Impact of power factor on faulty arm current. (a) T_1 fault. (b) T_2 fault. (Case 5 and case 6).

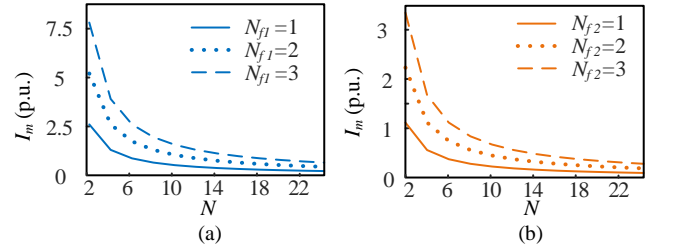


Fig. 9 Impact of number of faulty SMs on faulty arm current. (a) T_1 fault. (b) T_2 fault. (Cases 7-9).

and the power factor. To emphasize, the criterion in (15) and (19) are derived with certain simplification, and only the dominant impacts are included. There might be some errors compared to the actual operations since the control strategies, such as the circulating current control and the voltage balancing control, will also affect the faulty phenomenon. It provides a clue that when the unipolar arm current occurs and more measures will be taken to accelerate the fault location or avoid possible mislocation.

C. Impact factor of unipolar faulty arm current

According to the criterion in (15) and (19), the impact factors are analyzed in detail by drawing the curves to illustrate the tendency, as shown in Figs. 6-9, and the corresponding parameters of each case are shown in Table III.

Firstly, the curves of the I_m-N are drawn for different arm inductance in Fig. 6. All of the points on the curves indicate the critical operation condition of the unipolar faulty arm

current. Under the given number of SMs, the corresponding value of I_m indicates that the unipolar arm current could occur under smaller current or lower power. The higher I_m threshold indicates a higher risk of unipolar faulty arm current. With the increase of the SM quantity under the fixed DC bus voltage, the I_m threshold decreases, meaning that higher SM voltage is easier to trigger the unipolar arm current. The I_m threshold of T_1 and T_2 fault are both increased when the arm inductance is decreased from 8 mH to 5 mH. Comparing Fig. 6(a) and Fig. 6(b), it shows that the I_m threshold of T_1 fault is higher than T_2 . In other words, the faulty arm current of T_1 fault is easier to be unipolar under the same AC current level.

Secondly, the curves of the I_m - N are compared under $m=0.9$ and $m=0.8$ in Fig. 7. Even though the decrease of modulation index will increase the I_m threshold, the impact is slight, especially in the case of the high number of SMs. Note that the carrier frequency in case 3 and case 4 is increased to 2 kHz compared to case 1 and case 2. In Table III, case 1 and case 3 can be used to compare the influence of carrier frequency, which are curved as the solid lines in Fig. 6 and Fig. 7. Obviously, the increase of carrier frequency reduces the I_m threshold decreases the I_m threshold.

Thirdly, the influence of the power factor is displayed in Fig. 8. It shows that the reactive power can help to reduce I_m threshold and reduce the unipolar risk under faulty T_1 or T_2 .

Finally, the multiple SM faults with the same type of fault are shown to have high risk of causing unipolar arm current, as seen in Fig. 9 where higher number of faulty SMs produces higher I_m threshold.

Above all, the increase of faulty SM quantity and power factor will increase the risk of unipolar arm current; however, the increase of modulation index, carrier frequency, and arm inductance will decrease the risk of unipolar arm current. Under the fixed DC bus voltage, the decrease of SM quantity will increase the SM voltage, finally causing higher risk of unipolar arm current.

IV. PROPOSED FAULT LOCATION METHOD

A. Mechanism of faulty location

The existing software-based fault location methods are classified as three types, including the signal-, model-, and data-based methods. Basically, all of the methods are realized by distinguishing the faulty SM capacitor voltage with the healthy SM capacitor voltage. However, under the unipolar faulty arm current, the faulty and healthy SM capacitor voltage will rise or fall similarly. For example, the faulty arm current becomes nonnegative under T_1 fault, then all of the SM capacitors cannot be discharged and the faulty SM is hidden. Similarly, T_2 fault cannot be located under non-positive faulty arm current.

Therefore, to ensure that all of the existing approach can be well used without being degraded by the faulty unipolar arm current, the point is to produce bipolar arm current under T_1 or T_2 fault.

B. Proposed solution to unipolar arm current

This paper proposes the second-order circulating current injection approach as a solution to unipolar faulty arm current. The injected circulating current can rebuild the arm current to be bipolar so that the capacitor voltage deviations between the healthy and false SMs will be generated or enlarged during $i_{ap_f2}>0$ or $i_{ap_f1}<0$.

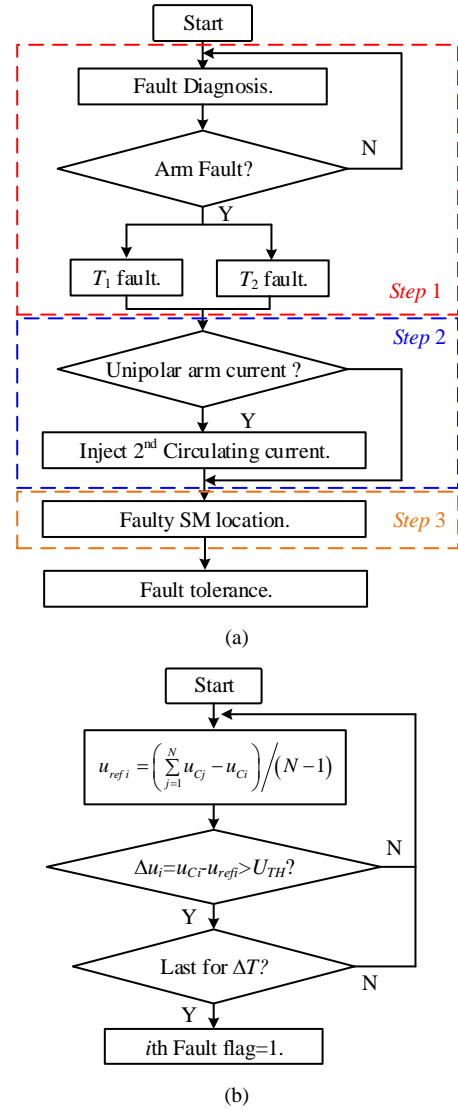


Fig. 10 Proposed fault location method under light load. (a) Enable of circulating current injection. (b) Fault location method.

Fig. 10 shows the implementation of the proposed fault location methods based on the circulating current injection. In Fig. 10(a), the fault location approach is performed in three steps.

Step 1: The fault diagnosis is performed to detect the faulty arm and type of faults. The approach in [13] can be directly used.

Step 2: The circulating current injection is only enabled after the arm fault is detected and the criterion in (15) or (19) is satisfied. The injected circulating current is given as

$$i_{2nd_x} = I_{2nd} \sin(\omega t + \varphi_x + \varphi_{2nd}) \quad (20)$$

where I_{2nd} and φ_{2nd} are the amplitude and phase of the second order circulating current, respectively. Specifically, the phase is determined by the fault type, i.e., T_1 or T_2 type, which is

$$\varphi_{2nd} = \begin{cases} -\frac{\pi}{2} & T_1 \text{ fault} \\ \frac{\pi}{2} & T_2 \text{ fault} \end{cases} \quad (21)$$

In this way, the missing negative/ positive interval of the faulty arm current could be compensated to the maximum extent. The amplitude of the injected second circulating current is decided by the current rating of the power device.

Table IV Simulation Parameters of MMC

Parameters	Value
DC voltage (U_{dc})	24 kV
AC Voltage Amplitude (U_m)	11 kV
Number of SMs (N)	12
Nominal Power (S)	7.5 MVA
SM Capacitance (C)	3 mF
Nominal SM Voltage (U_C)	2.0 kV

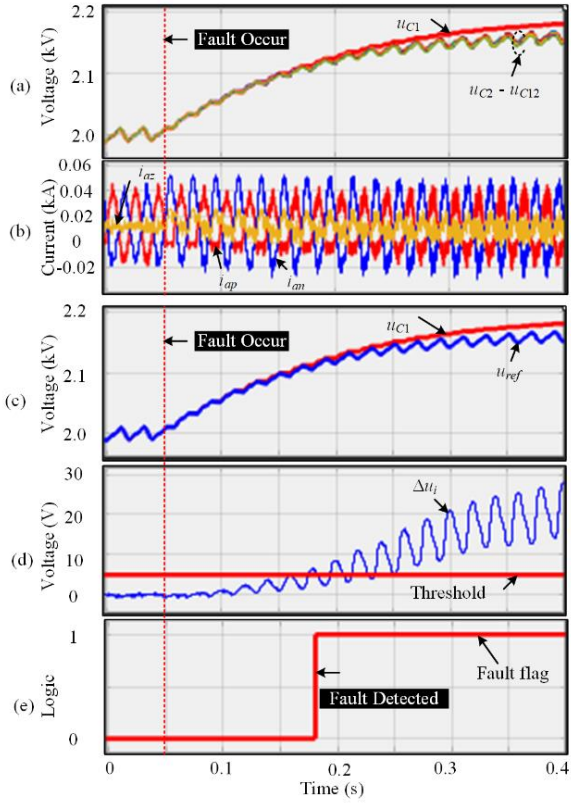


Fig. 11. Faulty SM location under T_1 fault and light load, without second order circulating current injection. (a) SM capacitor voltage. (b) Arm currents and circulating current. (c) SM1 capacitor voltage and reference value. (d) Comparison with threshold. (e) Fault flag of SM1.

Then the circulating current control in [14] is adopted to inject the second order circulating current; however, the injected circulating current cannot follow the reference value due to the false switching of the faulty SM. Nevertheless, the point is producing bipolar arm current rather than accurate circulating current track. Note that the healthy phase should also be compensated by the circulating current so that the DC link current will not be too severely distorted.

Step 3: After the circulating current is injected, the fault location is conducted, as shown in Fig. 10(b), where the classic method in [4] is adopted. The capacitor voltage of the detected SM is compared with the average voltage of the rest SMs u_{refi} , and the calculated voltage deviation Δu_i is compared with the given threshold U_{TH} . If $\Delta u_i > U_{TH}$ lasts for ΔT , then SM i can be detected as faulty SM and bypassed by the outer bypass breaker. ΔT is set as 5 ms in this paper.

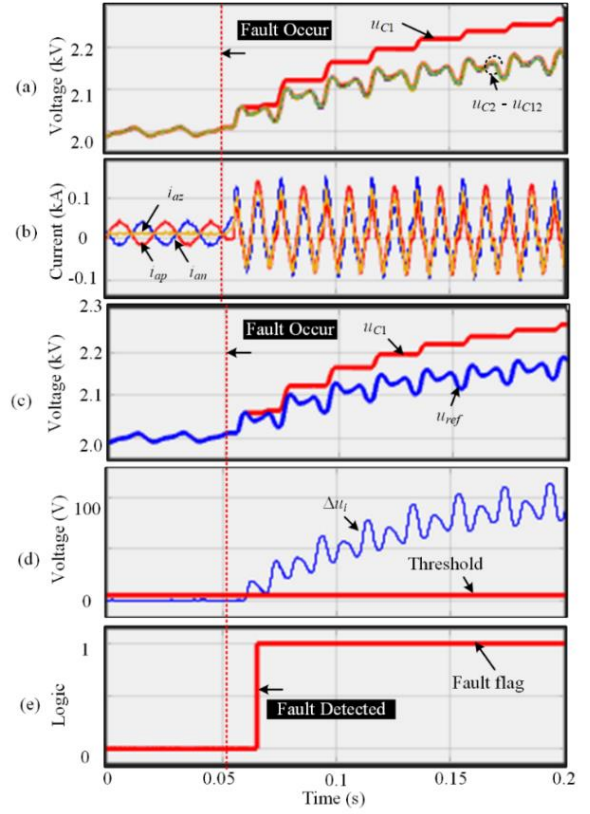


Fig. 12. Faulty SM location under T_1 fault and light load, with second-order circulating current injection. (a) SM capacitor voltage. (b) Arm currents and circulating current. (c) SM1 capacitor voltage and reference value. (d) Comparison with threshold. (e) Fault flag of SM1.

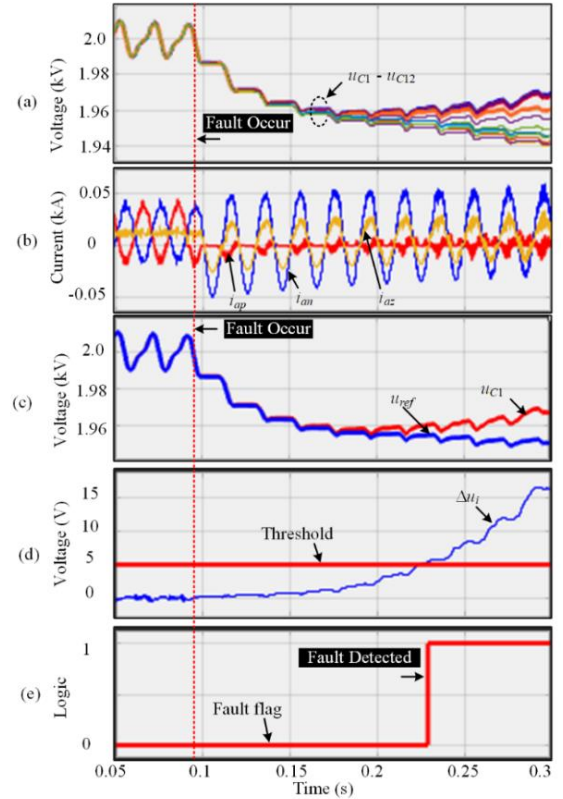


Fig. 13. Faulty SM location under T_2 fault and light load, without second order circulating current injection. (a) SM capacitor voltage. (b) Arm currents and circulating current. (c) SM1 capacitor voltage and reference value. (d) Comparison with threshold. (e) Fault flag of SM1.

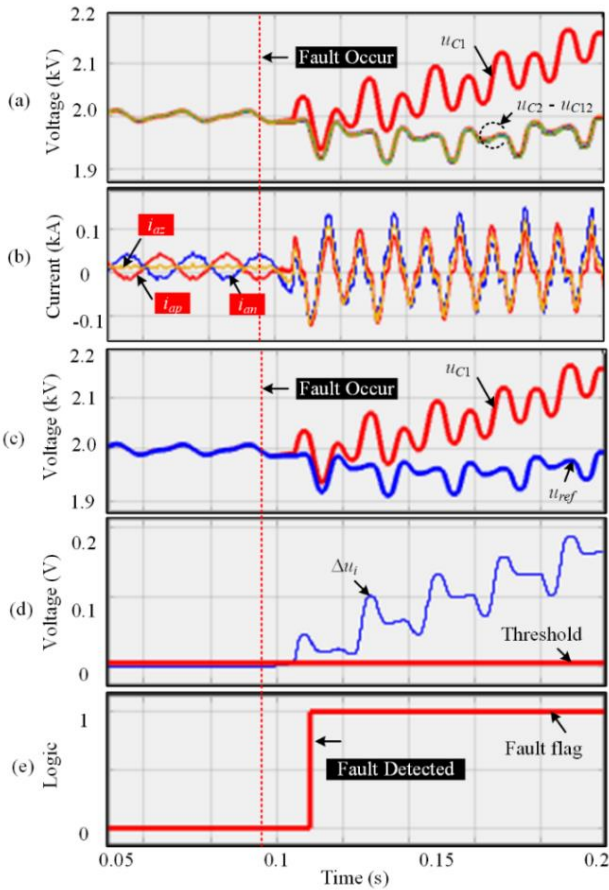


Fig. 14. Faulty SM location under T_2 fault and light load, with second order circulating current injection. (a) SM capacitor voltage. (b) Arm currents and circulating current. (c) SM1 capacitor voltage and reference value. (d) Comparison with threshold. (e) Fault flag of SM1.

Table V Fault location time under light load condition

Fault case	Circulating current injection	
	Without	With
T_1 fault	130 ms	17 ms
T_2 fault	135 ms	20 ms

V. VERIFICATIONS

The simulation verifications are carried out in Simulink/Matlab on a three-phase MMC with the parameters shown in Table IV. The carrier phase shift-based pulse width modulation approach is adopted to realize the voltage balancing for individual SM. The SM1 in the upper arm of phase a is assumed to be faulty. The simulation results are presented for the T_1 and T_2 fault under the power level $P=750$ kW (0.1 p.u.) with $I_m=50$ A. According to the given criterion in (15) and (19), the arm current will suffer from unipolarity under both T_1 and T_2 faults.

A. T_1 fault

Fig. 11 shows the SM fault location process under T_1 fault, where no extra measurement is taken. After the fault occurrence at $t=0.04$ s, the SM capacitor voltage in Fig. 11(a) is almost the same before $t=0.16$ s. The arm current of the fault upper arm in Fig. 11(b) is nearly unipolar, having only positive intervals. As a result, the voltage deviation between u_{C1} and u_{ref1} increases slowly and finally exceeds the threshold at $t=0.17$ s, where the threshold value is 5 V. Lasting for 10

ms, the fault flag of SM1 is turned to one, and the faulty SM is detected. The fault location time is 130 ms.

In Fig. 12, the proposed approach of second-order circulating current is employed for the fault location of T_1 . The fault occurs at $t=0.05$ s, and the detection time of the faulty arm is assumed to be 10 ms. Therefore, the circulating current injection is enabled at 0.06 s. It is shown in Fig. 12(a) that the voltage deviations between the healthy and faulty SM capacitors are enlarged by the circulating current injection. The voltage deviation Δu_i in Fig. 12(d) rises quickly, and the fault is located at $t=0.67$ s. Compared with Fig. 11, the fault location process is accelerated, and the location time is significantly reduced from 130 ms to 17 ms.

B. T_2 fault

Fig. 13 and Fig. 14 show the fault location under T_2 fault and light load when the circulating current injection is disabled and enabled, respectively.

It is shown in Fig. 13 that, after the fault happens at $t=0.95$ s, the positive interval of the faulty arm current is suppressed to almost zero, and the SM capacitor voltage is all decreased without apparent deviations. Then Δu_1 rises quite slowly and cannot reach the threshold until $t=0.22$ s. As a result, the faulty SM is located at $t=0.23$ s. The fault location time is 135 ms.

In Fig. 14, the second-order circulating current is injected at $t=0.1$ s, and the arm current becomes bipolar. Then the faulty SM capacitor voltage rises fast because it cannot be bypassed under positive arm current. As a result, Δu_1 rises quickly to surpass the threshold, and the fault is located at $t=0.11$ s. The fault location time is shortened to 20 ms.

Table V compares the fault location time with and without circulating current injection for the two types of faults. It justifies the effectiveness of the proposed approach of second-order circulating current injection.

VI. CONCLUSION

This paper proposes a non-invasive fault location method for MMC to accelerate the fault location process under the light load operation. The arm current is suppressed to be unipolar when the open-circuit fault happens on the SM switch under light load. The approach of injecting the second-order circulating current will rebuild the bipolar arm current and enlarge the capacitor voltage deviations between the healthy and faulty SMs. As a result, the fault location time is significantly shortened. The simulations are carried out to validate the effectiveness of the proposed approach, presenting that the fault location time is reduced to 1/6 compared with the condition without using the second-order circulating current injection.

Also, considering possible negative impacts, the second order circulating current should be injected not surpassing five fundamental periods, which are sufficient to locate the faulty SMs by the proposed approach. Note that the proposed approach is only an improvement before the implementation of the fault location, so it is suitable for all of the existing fault location principles.

REFERENCES

- [1] H. Akagi, "Multilevel converters: Fundamental circuit and systems," *Proc. IEEE*, vol. 105, no. 11, pp. 2048–2064, Nov. 2017.
- [2] S. Shao, P. W. Wheeler, J. C. Clare, and A. J. Watson, "Fault detection for modular multilevel converters based on sliding mode observer," *IEEE Trans. Power Electron.*, vol. 28, no. 11, pp. 4867–4872, Nov. 2013.
- [3] S. Shao, A. J. Watson, J. C. Clare, and P. W. Wheeler, "Robustness analysis and experimental validation of a fault detection and isolation

- method for the modular multilevel converter,” *IEEE Trans. Power Electron.*, vol. 31, no. 5, pp. 3794–3805, May 2016.
- [4] F. Deng, Z. Chen, M.R.Khan, and R.Zhu, “Fault detection and localization method for modular multilevel converters,” *IEEE Trans. Power Electron.*, vol. 30, no. 5, pp. 2721–2732, May 2015.
- [5] W. Zhou, J. Sheng, H. Luo, W. Li, and X. He, “Detection and localization of submodule open-circuit failures for modular multilevel converters with single ring theorem,” *IEEE Trans. Power Electron.*, vol. 34, no. 4, pp. 3729–3739, Apr. 2019.
- [6] X. Chen, J. Liu, Z. Deng, S. Song, S. Du, and D. Wang, “A Diagnosis Strategy for Multiple IGBT Open-Circuit Faults of Modular Multilevel Converters,” *IEEE Trans. Power Electron.*, vol. 36, no. 1, pp. 191–203, Jan. 2021.
- [7] R. Picas, J. Zaragoza, J. Pou, and S. Ceballos, “Reliable Modular Multilevel Converter Fault Detection With Redundant Voltage Sensor,” *IEEE Trans. Power Electron.*, vol. 32, no. 1, pp. 39–51, Jan. 2017.
- [8] J. Zhang, X. Hu, S. Xu, Y. Zhang, and Z. Chen, “Fault Diagnosis and Monitoring of Modular Multilevel Converter With Fast Response of Voltage Sensors,” *IEEE Trans. on Indus. Electron.*, vol. 67, no. 6, pp. 5071–5080, Jun. 2020.
- [9] Q. Yang, J. Qin, and M. Saeedifard, “Analysis, Detection, and Location of Open-Switch Submodule Failures in a Modular Multilevel Converter,” *IEEE Trans. on Power Delivery*, vol. 31, no. 1, pp. 155–164, Feb. 2016
- [10] B. Li, S. Shi, B. Wang, G. Wang, W. Wang, and D. Xu, “Fault Diagnosis and Tolerant Control of Single IGBT Open-Circuit Failure in Modular Multilevel Converters,” *IEEE Trans. on Power Electron.*, vol. 31, no. 4, pp. 3165–3176, Apr. 2016.
- [11] S. Kiranyaz, A. Gastli, L. Ben-Brahim, N. Al-Emadi, and M. Gabbouj, “Real-time fault detection and identification for MMC using 1-D convolutional neural networks,” *IEEE Trans. Ind. Electron.*, vol. 66, no. 11, pp. 8760–8771, Nov. 2019.
- [12] C. Liu, F. Deng, X. Cai, Z. Wang, Z. Chen, and F. Blaabjerg, “Submodule Open-Circuit Fault Detection For Modular Multilevel Converters Under Light Load Condition With Rearranged Bleeding Resistor Circuit,” *IEEE Trans. Power Electron.*, vol. 37, no. 4, pp. 4600–4613, Apr. 2022.
- [13] Y. Jin et al., “A Novel Detection and Localization Approach of Open-Circuit Switch Fault for the Grid-Connected Modular Multilevel Converter,” *IEEE Trans. Ind. Electron.*, Early Access, doi: 10.1109/TIE.2022.3153810.
- [14] Z. Li, P. Wang, Z. Chu, H. Zhu, Y. Luo, and Y. Li. “An Inner Current Suppressing Method for Modular Multilevel Converters,” *IEEE Trans. Power Electron.*, vol. 28, no. 11, pp. 4873–4879, Nov. 2013.